

Ultrathin wide-bandgap a-Si:H based solar cells for transparent PV applications

Alex J. Lopez-Garcia, Oriol Blazquez, Cristobal Voz, Joaquim Puigdollers, Víctor Izquierdo-Roca, Alejandro Pérez-Rodríguez*

Alex J. Lopez-Garcia, Dr. Oriol Blazquez, Dr. Víctor Izquierdo-Roca, Prof. Alejandro Pérez-Rodríguez
Institut de Recerca en Energia de Catalunya (IREC), Jardins de les Dones de Negre, 1, 2^a pl,
08930, Sant Adrià del Besòs, Barcelona, Spain
E-mail: alopez@irec.cat

Dr. Cristobal Voz, Prof. Joaquim Puigdollers,
Departament Enginyeria Electrònica, Universitat Politècnica Catalunya, c/ Jordi Girona 3-1,
Barcelona, 08034, Spain

Prof. Alejandro Pérez-Rodríguez
IN²UB, Departament d'Enginyeria Electrònica i Biomèdica, Universitat de Barcelona, Carrer
de Martí i Franquès 1, 08028, Barcelona, Spain

Keywords: transparent photovoltaics, a-Si, UV-selective solar cells, selective contacts, oxides

This work reports the fabrication of UV-blue selective transparent solar cells based on ultrathin (<30 nm) intrinsic hydrogenated amorphous silicon films (a-Si:H) as absorber and using a fully inorganic architecture, using metal-oxide thin films as carrier selective contacts and as transparent electrical contacts. These transparent ultrathin devices present PV effect and high average visible transmittance (AVT), showing their potential as candidates for implementation as a transparent energy harvester. Potential applications range from Building-Integrated PV (BIPV) to agrophotovoltaics (APV), and can also be of interest as a ubiquitous and inexpensive power source integrated in functional devices such as low-power devices, IoT devices and other sensors. Glass/FTO/ZnO/a-Si:H/MoO₃/ITO device prototypes have been produced. These devices present an AVT ranging from 50% to 69%, present photovoltaic effect with a power conversion efficiency (PCE) up to 0.5% calculated for an AM1.5G spectrum and have light utilization efficiency (LUE) values of 0.25%, confirming the potential of the proposed device architectures for the development of highly transparent devices with improved LUE.

1. Introduction

There is no denying on the fact that solar energy has already attained a main role as a sustainable and renewable energy source in the energy mix of many countries in the last years. PV technologies opened the possibility of providing clean energy in a wide array of settings, focusing on the deployment of vast solar arrays or farms, while some others in more local settings, such as in buildings, in order to provide on-site energy. Conventional PV technologies suffer some important drawbacks that limit the possibility of using solar energy as the main energy source to power many different and diverse applications. Main issues are: usage of very large areas of land, high visual impact, weight, costs, raw material availability, limited efficiencies, environmental impact and low stability, amongst others, which depend on the kind of PV technology. Due to these facts, in order to expand the PV industry, it seems quite relevant to try to extend the range of applications and implementations of photovoltaic technologies. It is thus important to look back into what has been done and create new concepts that are applicable and translatable to the industry.

In the last years, increasing efforts have been made to obtain semi-transparent and fully transparent PV (TPV) devices that can be integrated in window façades. Building-Integrated PV (BIPV) applications are a clear example aiming to obtain near-zero emission buildings with solar cells fully integrated components of the building.^[1–5] Other novel applications include agrophotovoltaics (APV) and application as devices that could be integrated as functional components to power mid and low power optoelectronic devices such as sensors, electrochromic windows, as a multifunctional harvester and optical filter, as indoor light harvesters or IoT devices.^[6–11]

For transparent PV applications maximal efficiency is not the key premise for massive deployment. Instead other aspects such as visual impact, low cost and stability play an important role in their viability. For example, it will be more feasible (and practical) to integrate a solar cell in a glass façade if it does not disturb the building visual aspect (i.e. integration has greater potential for a transparent PV cell that reaches 10% efficiency than to attach 25% silicon PV modules and leave gaps in the windows). TPV devices can either be wavelength selective or non-selective, and have been fabricated with different absorber materials and device architectures.^[12–14]

As for inorganic wavelength-selective based devices, oxide and chalcogenide materials are very interesting for the development of this technology as they are stable, inexpensive, abundant, easy to process at industrial scale and typically non-toxic. State of the art inorganic UV-selective solar cells are mainly based on the use of ZnO or Zn(O,S) as the absorber material, but even though presenting high average visible transparency (AVT) values, they still have to overcome an efficiency limited to around 0.5%.^[15–19] However, recently, there have been demonstrations on implementing a-Si:H in UV-selective metal-oxide based solar cells, showing the possibility to overcome this PCE limitation, but at the cost of losing some transparency.^[20] The use of a-Si based technologies in this emerging field of PV has added benefits in terms of the use of materials that are stable and durable, that are not deemed as critical raw. Besides, it allows for high-throughput and readily implementation in the already existing a-Si industry and additionally, the low-temperature used during processing allows for device implementations in alternative substrates, ranging from rigid substrates such as metallic or glass-based to flexible substrates such as PET.^[21] These features highlight the versatility of this TPV application.

In this work transparent PV cells based on ultrathin intrinsic a-Si:H and oxide-based charge transport layers (CTLs) are presented. It is shown that it is possible to tune the AVT and PCE as a function of the a-Si:H absorber thickness. A study of the effect of the different

CTLs in the structure is presented. It is demonstrated that these cells absorb light in the UV range and in the blue range, by making the absorber ultrathin to increase its visual transparency at longer wavelengths. Optical and electrical properties of the fabricated devices are analysed and discussed here-in.

2. Results and Discussion

In the present work TPV devices have been fabricated using a structure consisting of Glass/FTO/ETL/a-Si:H/HTL/ITO. (**Figure 1**) Note that the ETL and HTL layers in this structure replace the n-doped and p-doped layers of classical p-i-n solar cells, respectively. FTO and ITO act as transparent electrodes, ultrathin intrinsic a-Si:H works as the absorber layer. As carrier selective contacts, metal-oxide ZnO (ETL: electron transport layer) and MoO₃ (HTL: hole transport layer) have been explored. These materials have already been studied as CTLs for conventional c-Si and a-Si:H technologies, as well as other technologies, due to its wide-bandgap, stability, material availability and low-cost. [22–24]

Traditionally, a-Si:H conventional (opaque) devices rely on forming either a p-i-n homojunction using doped a-Si:H or heterojunction using a-SiC:H as CTL.[25,26] In this particular application, we stress that the visual aspect and transparency are critical features. Given the direct bandgap of a-Si:H (ranging from 1.8 to 2.1 eV) and its relatively high absorption coefficient, the parasitic absorption in these functional charge-selective films is an aspect to be avoided, leading thus to this change in architecture implementing metal-oxide alternatives.[27–29] In terms of electrical properties, photogenerated carriers in the a-Si:H absorber have a rather short diffusion length.[30–32] However, given that we work with an ultrathin absorber, charge carrier collection in this case can easily occur, so photogenerated carriers will reach the interfaces with the metal-oxide selective contacts. This highlights an important aspect of these cells, which is the need of effective defect passivation, especially at the interfaces a-Si:H/CTL. Finally, the absorber thickness will also have a paramount impact

on both PCE and AVT, placing an effective trade-off between both parameters as a function of the thickness of the absorber, which will be discussed also.

Following optoelectronic characterization, we begin by analyzing the ZnO ETL and its impact on the device functionality. Then we study the impact of the MoO₃ HTL. Afterwards, after selecting the CTL materials and their thickness we turn the focus into the effect of the ultrathin absorber film and its impact on TPV parameters, mainly in terms of AVT, color rendering index (CRI), PCE and LUE. All these aspects are discussed here-in.

2.1. Analysis of the impact of the electron and hole selective contacts and absorber thickness

2.1.1. ZnO ETL

Recently, some studies have presented UV-selective metal-oxide/a-Si:H based TPV lab cells that incorporate NiO as HTL and thick ZnO film that also absorbs some UV radiation.^[20] The a-Si:H film was incorporated in order to improve electrical transport at the interface ZnO/NiO. Instead, it also seems to work as an absorber, as it is shown throughout this work. The referenced report showed that a 400nm ZnO acted as a UV absorber. However, an efficient ETL is usually made with thinner materials, typically of few nanometers in thickness, giving that carrier collection relies on tunneling mechanisms if their work-function is adequate respect to the absorber energy bands.

With this in mind this work has studied the implementation of ZnO as an effective ETL in the a-Si:H system. The study consisted on using a 15 nm intrinsic a-Si:H absorber and a fixed HTL thickness and testing devices with different ZnO thickness: 0 nm, 50 nm and 400 nm. The device structure is SLG/FTO/ZnO/a-Si:H(15nm)/MoO₃(20nm)/ITO. These devices have been characterized and J-V measurements have been carried out (**Figure 2a**).

Photovoltaic effect is obtained in all three cases. However, there are clear differences. While all three devices present a similar V_{OC}, FF and J_{SC} are clearly affected by the thickness of the

ETL. For the case of no ZnO layer (i.e. 0 nm) the shape of the curve in the first quadrant is almost a straight line from 0 V to V_{OC} . This suggests that some charges (electrons) absorbed in the ultrathin a-Si:H film can be collected as they can reach the interface with the FTO. However, the very low FF can indicate the presence of a barrier at this interface that increases recombination. By introducing the ZnO film with thickness of 50 nm an overall performance increase is observed. Notably J_{SC} and FF are enhanced, showing the need for an ETL that eases electron transport from a-Si:H to the electrical contact. However, if ZnO thickness is increased to 400 nm the photovoltaic parameters are impacted, and a reduction in performance is observed. This is attributed to a high resistance due to the intrinsic nature and high thickness of the fabricated ZnO film, causing a drop in J_{SC} and FF, as compared to the device with a 50 nm film. According to this, an optimized device using an Al doped ZnO (AZO) layer as ETL has been produced and is discussed in section 2.2.

2.1.2. MoO_3 HTL

Same as for the ETL case, it is worth moving towards HTLs with a wide bandgap, higher than 3 eV, in order to increase device transparency and reduce visual impact. In this work MoO_3 is studied as hole transport layer. MoO_3 presents a wide bandgap of 3.2 eV and a high work function, which makes it a good hole selective contact.

Similarly, different thicknesses have been explored: 0, 10 and 20 nm. Absorber thickness and ETL thickness were fixed to 15 nm and 50 nm respectively. From the current-voltage characteristics the influence of the material and its thickness on the photovoltaic parameters of the devices is assessed. (**Figure 2b**)

The device with no MoO_3 presents almost no PV effect whatsoever, signaling the need of a HTL in order to promote hole collection at the front contact. When a 10 nm MoO_3 film is introduced in the device structure PV effect is clearly observed, showing in this case a V_{oc} close to 0.3 V. Fill factor is quite low, 30%, indicating high series resistance and low shunt

resistance. When a 20 nm MoO₃ film is used the efficiency is almost the same, with a similar J_{SC} of the device with 10nm film. However, FF and V_{OC} are slightly different. For the 20nm films an anomaly in the conventional exponential shape of the current-voltage curve is observed. This anomaly has been discussed already in literature in both organic and inorganic PV materials and is dubbed as s-shape, kink, or roll-over.^[33–39] The impact on PV parameters is basically a reduction in FF due to a dampening of the exponential current flow with increasing voltage up to a given value where the single exponential character is recovered. These lead to a lower maximum power point than for a device without such s-shape. It can be observed that FF is reduced but V_{OC} slightly increases as compared to the case of a 10 nm MoO₃ film. Overall, the efficiency is almost the same.

The MoO₃ films are deposited by thermal evaporation at ambient temperature and were exposed to air. It has been reported that air exposed MoO₃ films present a reduced WF of 5.4 eV as compared to films unexposed to air, reported at 6.8 eV.^[22,40,41] Hole transport in MoO₃ has been studied in both organic and inorganic PV technologies. Even though presenting n-type conductivity the material yields efficient hole transport. Concretely, in a-Si:H devices, the conduction band of MoO₃ is reported to be lower than the valence band of a-Si:H leading to band-to-band tunneling transport. However, if the WF is not low enough, a barrier will form. In this case the transport is also mediated by gap-states through trap-assisted tunneling. These gap-states have been attributed to oxygen vacancies and give rise to its conductivity. The height of the barrier formed at the interface a-Si:H/MoO₃ will heavily depend on the WF of the MoO₃. Thus, WF is a critical parameter affecting carrier selectivity.^[42–45]

In this work, the loss of selectivity observed for the thicker MoO₃ HTLs could be attributed to two factors. The first one is the mentioned barrier due to the reduced WF due to air-exposure. In this case, the hole selectivity relies on efficient tunneling via gap-states. The thicker film will possess higher resistance and recombination at the film will occur as charge accumulates, leading to the roll-over effect. However, for the 10nm film the curve presents a conventional

exponential shape, indicating good hole selectivity, suggesting the use of even thinner films if these present excellent coverage. Nonetheless, for both film thicknesses, FF and V_{OC} present quite low values. Given the nanometric thickness of the films present in the device, it is expected that interfaces play a critical part in device functionality. It is critical to minimize energy barriers at the interfaces to have good carrier extraction. Besides, a low-defect density and well passivated interfaces are needed in order to reduce interface recombination, as this will be the dominant non-radiative recombination mechanism (given that bulk effects can be neglected at these feature sizes). Hence, this can be a potential way to notably increasing device efficiency while maintaining similar or equal AVT values.

2.1.3. Analysis of the a-Si:H absorber thickness

After studying the effect of the charge transport layers, we aim at studying and optimizing the a-Si:H absorber thickness. In this work two absorber thickness values are investigated: 15 and 30 nm. The ZnO ETL is fixed to 50nm and two different thicknesses of 10 and 20 nm MoO_3 films are used as HTL, according to the results presented in the previous sections. This gives a total of four different device combinations (FTO/ZnO(50 nm)/a-Si:H(15,30 nm)/ MoO_3 (10,20 nm)/ITO). In order to have representative results that can be compared we make device production in parallel. Thus a single deposition of ZnO is done, then two devices are subjected to the 15 nm a-Si:H deposition and the other two to the 30 nm deposition. Later one 15 nm and one 30 nm device are subjected to a 10 nm MoO_3 deposition and the remaining pair of devices to the 20 nm MoO_3 deposition. Finally, a single ITO deposition for all devices is carried out.

Subsequently, current-voltage measurements under AM1.5G illumination have been carried out and will be discussed in this sub-section (**Figure 2c**).

Firstly, and continuing with the discussion of the previous sub-section, regardless of absorber thickness and ETL, an s-shaped profile is observed for devices with the 20nm MoO_3 HTL.

Focusing on effects related to the absorber thickness, it is observed that the photovoltaic parameters are improved overall for the thickest absorber regardless of the carrier selective contacts (**Table 1**). This is straightforward, given the fact that we are working with ultrathin nanometric films and that there is a forced absorption loss. Thus, in an ideal case, the expected result could be an effective doubling of J_{SC} . Experimental results show higher J_{SC} , almost double comparing the 30 nm against the 15 nm a-Si:H film (regardless of the HTL thickness). FF and V_{OC} also increase notably for the case of the 30 nm absorber, with values up to 41% and 0.46 V respectively.

2.2. Device architecture design of resulting TPV devices

In this section, the best devices are characterized by optical spectrophotometry, performing transmittance and reflectance measurements of the completed device structure. In the previous section, it was shown that the best results came from the use of a 50 nm ZnO film as ETL and a 10 nm MoO_3 film as HTL. Two devices with these CTLs and a-Si:H absorbers with thickness of 15 and 30 nm will be used, plus an additional device with a 15 nm absorber with a first optimization including a 75 nm AZO ETL film deposited by Atomic Layer Deposition. The J-V measurements under AM1.5G illumination of these devices are presented all-together in order to compare the two relevant performance indicators in TPV: PCE and AVT (**Figure 3; Table 2**).

Absorbance spectra of the three devices is presented in Figure 3b. The most notable feature is that for the devices with a 15 nm a-Si:H film there is a blue-shift in the absorption onset, as compared with the device with 30nm a-Si:H, suggesting an increase in the optical bandgap. The a-Si:H films present a reported direct bandgap of 1.8 eV in bulk, and it has also been reported to be extended up to 2.1 eV via quantum confinement, when film thickness is reduced to the nanometric scale.^[46] They also present a high absorption coefficient for

wavelengths with energy higher than its bandgap. A prototypical inorganic single-junction UV-TPV device should have its bandgap as close as the UV spectral onset, in order to totally avoid visible light absorption. This results in a rather natural wavelength selectivity. However, it is possible to mostly absorb UV light and some part of the blue-end spectrum with a-Si:H absorbers. By reducing the thickness to the nanometric scale there will be frustrated absorption of visible light and hence higher transparency. However, there will still be some visible light absorption and given the bandgap of the material, it will inevitably present some slight coloring albeit showing quite high AVT values (It is worth noting that if AVT values are >50% it is possible to implement dichroic filters in order to tune the color aspect and effectively reducing it at the cost of some AVT loss). This is observed in the absorbance spectra. For devices with 15 nm a-Si:H most of the absorption occurs below 500 nm, increasing absorption as wavelength is reduced. Same happens for the device with 30 nm a-Si:H, except that absorption is higher from 400 to 600 nm, when compared against the devices with 15 nm absorber. The devices with an optimized AZO film show higher absorption in the spectral range below 450 nm (i.e UV/blue).

The reflectance spectra, presented in Figure 3d shows that this is attributed to an important reduction in reflectance losses within this spectral range, highlighting the need for a careful optimization of the devices in terms of optical management, as subtle changes yield notable changes in parameters such as AVT, PCE and CRI. It is also noted that reflectance values (in the range above the absorber bandgap) are quite high, above 30%, signaling additional losses in device absorption that would not incur in reduced AVT. This is attributed to the fact that the FTO presents low roughness and thus it is expected that the nanometric films grown on top will accordingly present low roughness. Planar surfaces typically involve higher reflectance values than rough surfaces, given that optical indices of the materials remain unchanged. Additionally, differences seen in reflectance spectra comparing devices with 15 nm and 30 nm of a-Si:H are observed. This effect is very likely related to changes in optical

interference for the different layer thicknesses. On the other hand, slight variations in the properties of the material could not be discarded. Reducing these reflection losses will consequently increase the device PCE in a relative percentage that is proportional to these reflection losses.

Transmittance and reflectance spectra can be used to extract the AVT and CRI of the completed devices (for detailed information on AVT and CRI see ref. ^[12]). Optical transmittance and reflectance of the completed devices was measured from 300 nm to 800 nm range to assess the transparency and visual aspect of the TPV devices. LUE is then finally calculated from multiplying AVT and PCE, in order to complete the TPV characterization. All these parameters are summarized in Table 2.

AVT values for these devices ranged from 50% to 69%. Interestingly, the AVT drastically changed in-between 15 nm a-Si:H based devices when changing from a 50 nm ZnO film to a 75 nm AZO layer. The device with the ZnO film shows an AVT=69%, a CRI=89 ($a^*=-0.18$, $b^*=21$) and PCE=0.21%, yielding a LUE=0.15%. The device with the AZO layer shows an AVT=62%, CRI=79 ($a^*=4$, $b^*=31$) and PCE=0.41%, yielding a notably higher LUE=0.25%. This increase is basically due to the overall improved PV performance. The doped AZO layer grown by ALD yields higher FF and V_{OC} , probably due to increased doping which impacts on the increased V_{OC} . Most notably, there is a remarkable increase in J_{SC} when compared to the device with ZnO. In fact, it is almost the same as for the device with a thicker 30 nm a-Si:H absorber, suggesting a beneficial impact in both electrical and optical management. However, this increase in performance came as a reduction in AVT and more notably in CRI. The device with ZnO and a “thick” 30 nm layer presents an AVT=50%, CRI=74 ($a^*=2.67$, $b^*=21$) and PCE=0.51%, yielding a LUE=0.25%. Even though LUE is the same as for the device with a 15 nm a-Si:H film with a 75 nm AZO ETL, the visual aspect differs notably, presenting the former lower AVT and CRI values.

These results highlight that very subtle differences in device structure have much higher impact in TPV technologies compared to conventional opaque PV. This is caused by the inevitable trade-off between efficiency and transparency, with the add-on of visual aspect. It is concluded that depending on the specific application requirements and constraints, different devices could be selected if given a catalogue showing these three devices. For example, for low power applications with a high demand on color-neutrality and high transparency the device with lower LUE with high CRI and AVT may be adequate, as constraint is more pressing on visual aspect. This remarks also that when working with transparent technologies with bandgaps that lie within the visible range, like in this case, it is relevant to present, if possible, devices with different ratio AVT/PCE, to test the limits of a given TPV technology in terms of the trade-off AVT/PCE (i.e. highest PCE with lower AVT and highest AVT at cost of reduced PCE).

Finally, when assessing the photovoltaic parameters extracted from the J-V measurements (see Figure 3a and Table 2), different conclusions can be observed. First, comparing the devices with a 15 nm a-Si:H absorber we see that the optimized AZO film leads to an overall improvement. Notably, FF increases from 31 to 41.4 % when switching the ZnO film by an AZO film, a relative increase of 20%. J_{SC} increases from 1.85 to 2.86 mAcm^{-2} , a relative increase of 55% without changing the absorber thickness. In terms of V_{OC} , a relative increase of 48% is observed, going from 0.29 V to 0.43 V (even higher than for the device with an absorber thickness of 30 nm). An antireflective coating in the UV/blue range would further increase the PCE by increasing absorption in this spectral range.

3. Conclusion

We have studied the potential use of ultrathin intrinsic a-Si:H as a potential wavelength-selective absorber for inorganic TPV applications in a device architecture including highly

transparent metal-oxide carrier selective contacts and using transparent conductive oxides as electrical contacts. We have shown that ZnO acts as ETL and MoO₃ as HTL, and the impact of the thickness of the different layers in the device architecture has been analyzed, showing the possibility to achieve devices with values of AVT in the range from 50% to 69% and AM1.5G power conversion efficiencies up to 0.5%, corresponding to LUE values up to 0.25%. We have shown that by using an ultrathin a-Si absorber layer devices are engineered to allow for wavelength selectivity in the UV to blue wavelength ranges, with the existence of a trade-off behavior between PCE and AVT with the a-Si layer thickness. On the other hand, replacement of the ZnO CTL by AZO layers leads to a relevant improvement of the optoelectronic characteristics of the devices when compared to solar cells with similar a-Si absorber thickness. Estimation of the device parameters using FTO/AZO/a-Si/MoO₃/ITO optimized architectures gives expected efficiency values higher than 1%, with a relevant improvement in relation to state-of-the-art devices. Future optimizations may involve the use of alternative (doped) metal-oxides such as TiO₂ and/or dipole layers such as LiF as ETL. These structures show a promising route for alternative applications and as a ubiquitous power source for low-power devices that can effectively extend the range of applications within the photovoltaic area. In order to increase PCE it becomes relevant to perform an in-depth characterization of interfaces, as they might be critical in efficiency, especially for such an ultrathin inorganic nanodevice (around 100 nm, excluding TCO electrical contacts). The benefit is that by carefully tuning these interfaces there will not be any impact in the visual aspect of the TPV device, which is a parameter of utmost importance. An added benefit of these devices are that all materials and processes are scalable and compatible with existing and established industries, using earth-abundant, stable and low-cost materials.

4. Experimental Section/Methods

Sample Preparation: The solar cells fabricated in this work present the structure Glass/FTO/ZnO/a-Si:H(15, 30 nm)/MoO₃/ITO. Commercial Glass/FTO substrates (Merck; $R_{sh}=13\ \Omega\text{sq}^{-1}$, AVT=83%, thickness of 250 nm) were used as substrate and transparent back-contact for the solar cell devices. Prior to deposition, substrates were first rinsed in distilled water, dried in Ar flux and afterwards cleaned by subsequent baths in isopropanol and milli-Q H₂O in an ultrasonic bath at room temperature for 10 min each and then were dried with Ar flux. Finally, they were subjected to a 5 min Ozone treatment. ZnO films were deposited by DC-Pulsed Magnetron Sputtering (Alliance CT-100). Prior to deposition the chamber was evacuated at 10^{-7} mbar. The ZnO target (Neyco; 4N) was pre-sputtered to remove any surface contaminants with the shutter in closed configuration. The deposition took place at room temperature with no intentional heating at a working pressure of $3\cdot 10^{-3}$ mbar in Ar atmosphere at 40 sccm, applying a DC power density of $1.8\ \text{Wcm}^{-2}$ to the target. Afterwards, intrinsic a-Si:H ultrathin films of either 15 nm or 30 nm were deposited by PE-CVD (Elettrorava) with an RF power supply of 13.56 MHz at 6W and at 400°C (measured substrate temperature at around 200°C) with a mix of SiH₄ and CH₄ at 36 and 12 sccm respectively. The deposition time was 2 minutes and 4 minutes for the a-Si:H films of 15 nm and 30 nm, respectively. MoO₃ films were deposited by thermal evaporation (Oerlikon Univex 250). MoO₃ powder (Alfa Aesar; 99.995%) was used as evaporant in a tungsten boat. The chamber was evacuated at a base pressure of 10^{-6} mbar before evaporation and the deposition took place at room temperature, with no intentional heating, at a rate of $0.5\ \text{\AA s}^{-1}$ measured with a quartz crystal microbalance (Inficon SQC-310; Ag 6 MHz sensor). To complete the device, a 190 nm thick ITO film was deposited by DC-Pulsed Magnetron Sputtering (Alliance CT-100). Prior to deposition the chamber was evacuated at 10^{-7} mbar and the substrate was heated up to 200 °C. The ITO target (Neyco; In₂O₃/SnO₂ 90/10 wt%, 4N) was pre-sputtered to remove any surface contaminants with the shutter in closed configuration. The deposition took place at 200 °C

(nominal) at a working pressure of $3 \cdot 10^{-3}$ mbar in a mixed Ar/O₂ atmosphere at 30/0.5 sccm, applying a DC power density of 1.9 Wcm^{-2} to the target. For the optimized device with an AZO ETL, a 75 nm film was grown in an ALD system (Savannah S200, Cambridge Nanotech) at 135°C. The precursors used are Diethylzinc (DEZ), ultrapure H₂O and Trimethylaluminium (TMA) and using N₂ as purging gas, with a DEZ:TMA ratio of 19:1. 21 supercycles were performed with 19 H₂O/N₂/DEZ/N₂ (20 ms/3 s/15 ms/3 s) cycles and 1 H₂O/N₂/TMA/N₂ (50 ms/1 s/20 ms/5 s) cycle.

Characterization: UV-VIS measurements were acquired with a dual-beam spectrophotometer setup (Perkin Elmer Lambda L950) in Transmittance and in Reflectance mode (with an integrating sphere) from 300 to 800 nm.

J-V (current density-voltage) measurements under illumination were carried out using a AAA solar simulator with AM1.5G illumination calibrated using a NREL-certified Si reference solar cell (Abet Technologies Model 15150). Electrical measurements were carried out with a source-measure unit (Keithley SMU 2400) in 4-wire sense mode, controlled by the software Tracer (ReRa solutions) using a IEEE 488 GPIB Instrument Control Device (National Instruments GPIB-USB-HS). For these optoelectronic measurements the sample was measured with a mask and has been placed in a dark opaque matt in order to avoid any back-reflections that could alter the characterization of the transparent solar cells.

Conflicts of interest

The authors declare that there are no conflicts of interest.

Acknowledgements

This work has received funding from the European Union H2020 Framework Programme under Grant Agreement no. 826002 (Tech4Win). Authors from IREC and Universitat de Barcelona belong to the SEMS (Solar Energy Materials and Systems) Consolidated Research Group of the “Generalitat de Catalunya” (Ref. 2017 SGR 862). Authors from UPC acknowledge and have received funding from MATER-ONE, MICINN-AEI PID2020-116719RB-C41 and SCALED, MICINN-AEI PID2019-109215RB-C41.

Received: ((will be filled in by the editorial staff))
 Revised: ((will be filled in by the editorial staff))
 Published online: ((will be filled in by the editorial staff))

References

- [1] A. Pérez-Rodríguez, presented in *NEXTGEN '19: 2019 Next Generation High Efficiency Photovoltaics International School and Workshop*, Mallorca, October **2019**
- [2] P. Heinstein, C. Ballif, L.-E. Perret-Aebi, *Green* **2013**, 3, 125.
- [3] F. J. W. Osseweijer, L. B. P. van den Hurk, E. J. H. M. Teunissen, W. G. J. H. M. van Sark, *Renew. Sustain. Energy Rev.* **2018**, 90, 1027.
- [4] E. Biyik, M. Araz, A. Hepbasli, M. Shahrestani, R. Yao, L. Shao, E. Essah, A. C. Oliveira, T. del Caño, E. Rico, J. L. Lechón, L. Andrade, A. Mendes, Y. B. Atlı, *Eng. Sci. Technol. an Int. J.* **2017**, 20, 833.
- [5] K. Lee, H. D. Um, D. Choi, J. Park, N. Kim, H. Kim, K. Seo, *Cell Reports Phys. Sci.* **2020**, 1, 100143.
- [6] E. P. Thompson, E. L. Bombelli, S. Shubham, H. Watson, A. Everard, V. D'Ardes, A. Schievano, S. Bocchi, N. Zand, C. J. Howe, P. Bombelli, *Adv. Energy Mater.* **2020**, 10, 2001189.
- [7] S. Schindele, M. Trommsdorff, A. Schlaak, T. Obergfell, G. Bopp, C. Reise, C. Braun, A. Weselek, A. Bauerle, P. Högy, A. Goetzberger, E. Weber, *Appl. Energy* **2020**, 265, 114737.
- [8] A. Agostini, M. Colauzzi, S. Amaducci, *Appl. Energy* **2021**, 281, 116102.
- [9] A. Brodu, C. Seydoux, G. Finazzi, C. Dublanche-Tixier, C. Ducros, *Thin Solid Films* **2019**, 689, 137492.
- [10] G. Kim, J. W. Lim, J. Kim, S. J. Yun, M. A. Park, *ACS Appl. Mater. Interfaces* **2020**, 12, 27122.
- [11] X. Lin, Y.-L. Loo, M. Sezen-Edmonds, N. C. Davy, J. Gao, A. Liu, A. Kahn, N. Yao,

- Nat. Energy* **2017**, 2, 17104.
- [12] C. J. Traverse, R. Pandey, M. C. Barr, R. R. Lunt, *Nat. Energy* **2017**, 2, 849.
- [13] F. Grifoni, M. Bonomo, W. Naim, N. Barbero, T. Alnasser, I. Dzeba, M. Giordano, A. Tsaturyan, M. Urbani, T. Torres, C. Barolo, F. Sauvage, *Adv. Energy Mater.* **2021**, 2101598.
- [14] Q. Xue, R. Xia, C. J. Brabec, H. L. Yip, *Energy Environ. Sci.* **2018**, 11, 1688.
- [15] D. K. Ban, M. Patel, T. T. Nguyen, J. Kim, *Adv. Electron. Mater.* **2019**, 5, 1.
- [16] M. Patel, H. S. Kim, J. Kim, J. H. Yun, S. J. Kim, E. H. Choi, H. H. Park, *Sol. Energy Mater. Sol. Cells* **2017**, 170, 246.
- [17] R. Karsthof, P. Racke, H. Von Wenckstern, M. Grundmann, *Phys. status solidi* **2016**, 213, 30.
- [18] R. Karsthof, H. von Wenckstern, M. Grundmann, *J. Vac. Sci. Technol. B, Nanotechnol. Microelectron. Mater. Process. Meas. Phenom.* **2016**, 34, 04J107.
- [19] A. J. Lopez-Garcia, A. Bauer, R. Fonoll Rubio, D. Payno, Z. Jehl Li-Kao, S. Kazim, D. Hariskos, V. Izquierdo-Roca, E. Saucedo, A. Perez-Rodrıguez, *Sol. RRL* **2020**, 4, 2000470.
- [20] S. Kim, M. Patel, T. T. Nguyen, J. Yi, C. P. Wong, J. Kim, *Nano Energy* **2020**, 77, 105090.
- [21] J. Ramanujam, D. M. Bishop, T. K. Todorov, O. Gunawan, J. Rath, R. Nekovei, E. Artegiani, A. Romeo, *Prog. Mater. Sci.* **2020**, 110, 100619.
- [22] L. G. Gerling, S. Mahato, A. Morales-Vilches, G. Masmitja, P. Ortega, C. Voz, R. Alcubilla, J. Puigdollers, *Sol. Energy Mater. Sol. Cells* **2016**, 145, 109.
- [23] L. Fang, S. J. Baik, K. S. Lim, *Thin Solid Films* **2014**, 556, 515.
- [24] J. Ding, Y. Zhou, G. Dong, M. Liu, D. Yu, F. Liu, *Prog. Photovoltaics Res. Appl.* **2018**, 26, 974.
- [25] D. E. Carlson, C. R. Wronski, *Appl. Phys. Lett.* **1976**, 28, 671.

- [26] T. Matsui, A. Bidiville, K. Maejima, H. Sai, T. Koida, T. Suezaki, M. Matsumoto, K. Saito, I. Yoshida, M. Kondo, *Appl. Phys. Lett.* **2015**, *106*, 053901.
- [27] K. Fukutani, M. Kanbe, W. Futako, B. Kaplan, T. Kamiya, C. . Fortmann, I. Shimizu, *J. Non. Cryst. Solids* **1998**, 227–230, 63.
- [28] A. S. Ferlauto, G. M. Ferreira, J. M. Pearce, C. R. Wronski, R. W. Collins, X. Deng, G. Ganguly, *J. Appl. Phys.* **2002**, *92*, 2424.
- [29] G. E. Jellison, F. A. Modine, *Appl. Phys. Lett.* **1996**, *69*, 371.
- [30] E. A. Schiff, R. I. Devlen, H. T. Grahn, J. Tauc, S. Guha, *Appl. Phys. Lett.* **1989**, *54*, 1911.
- [31] E. . Schiff, *Sol. Energy Mater. Sol. Cells* **2003**, *78*, 567.
- [32] E. A. Schiff, *J. Non. Cryst. Solids* **2006**, *352*, 1087.
- [33] A. Froitzheim, K. Brendel, L. Elstner, W. Fuhs, K. Kliefoth, M. Schmidt, *J. Non. Cryst. Solids* **2002**, 299–302, 663.
- [34] A. Gusain, R. M. Faria, P. B. Miranda, *Front. Chem.* **2019**, *7*, 61.
- [35] W. Tress, K. Leo, M. Riede, *Phys. Rev. B* **2012**, *85*, 155201.
- [36] W. Tress, O. Inganäs, *Sol. Energy Mater. Sol. Cells* **2013**, *117*, 599.
- [37] A. Wagenpfahl, D. Rauh, M. Binder, C. Deibel, V. Dyakonov, *Phys. Rev. B - Condens. Matter Mater. Phys.* **2010**, *82*, 1.
- [38] W. Tress, K. Leo, M. Riede, *Adv. Funct. Mater.* **2011**, *21*, 2140.
- [39] R. Saive, *IEEE J. Photovoltaics* **2019**, *9*, 1477.
- [40] J. Meyer, A. Shu, M. Kröger, A. Kahn, *Appl. Phys. Lett.* **2010**, *96*, 133308.
- [41] Irfan, H. Ding, Y. Gao, C. Small, D. Y. Kim, J. Subbiah, F. So, *Appl. Phys. Lett.* **2010**, *96*, 243307.
- [42] C. Liu, M. Cai, Y. Yang, Z. Arain, Y. Ding, X. Shi, P. Shi, S. Ma, T. Hayat, A. Alsaedi, J. Wu, S. Dai, G. Cao, *J. Mater. Chem. A* **2019**, *7*, 11086.
- [43] M. Kröger, S. Hamwi, J. Meyer, T. Riedl, W. Kowalsky, A. Kahn, *Appl. Phys. Lett.*

2009, *95*, 123301.

- [44] Y. Guo, J. Robertson, *Appl. Phys. Lett.* **2014**, *105*, 222110.
- [45] R. García-Hernansanz, E. García-Hemme, D. Montero, J. Olea, A. del Prado, I. Mártel, C. Voz, L. G. Gerling, J. Puigdollers, R. Alcubilla, *Sol. Energy Mater. Sol. Cells* **2018**, *185*, 61.
- [46] Y. Abdulraheem, I. Gordon, T. Bearda, H. Meddeb, J. Poortmans, *AIP Adv.* **2014**, *4*, 057122.

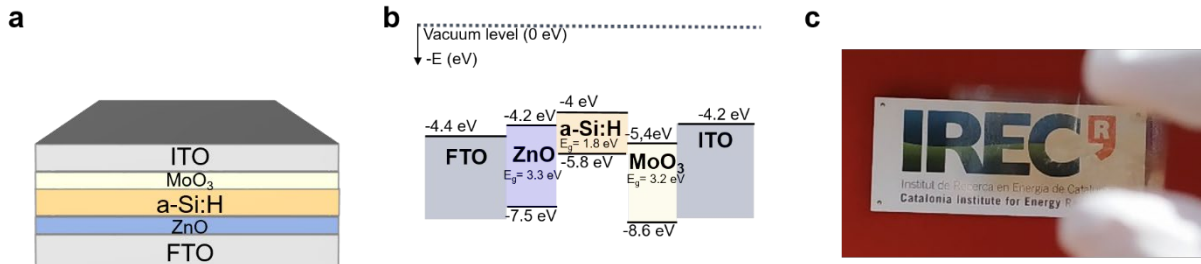


Figure 1. a) Schematic illustration of the TPV device architecture; b) Energy band diagram in equilibrium for the different nanometric films in the system. c) Picture taken outdoors in broad daylight. The picture shows the TPV device, showing a white board with the IREC logo located at the building entrance.

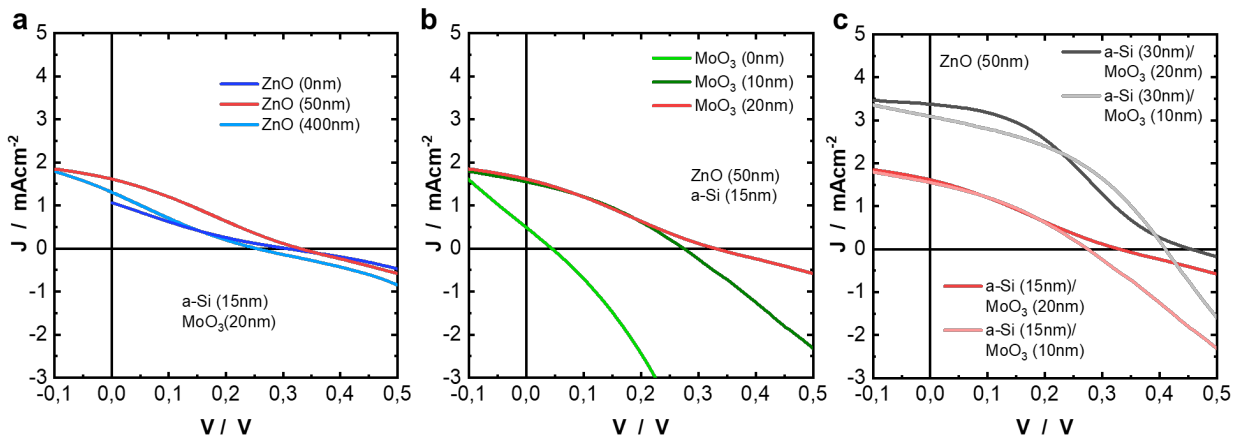


Figure 2. Photovoltaic characterization of fabricated TPV devices. a) J-V measurements under AM1.5G illumination of a device with a 20 nm MoO₃ HTL and a 15 nm a-Si:H absorber with different ETL thickness. b) J-V measurements for a 15 nm a-Si:H absorber and a 50 nm ZnO ETL, with different HTL thickness. c) J-V measurements of devices with varying a-Si:H thickness with a fixed 50 nm ZnO ETL. For each a-Si:H thickness, for comparison, there are two MoO₃ films with 10 nm and 20 nm thicknesses.

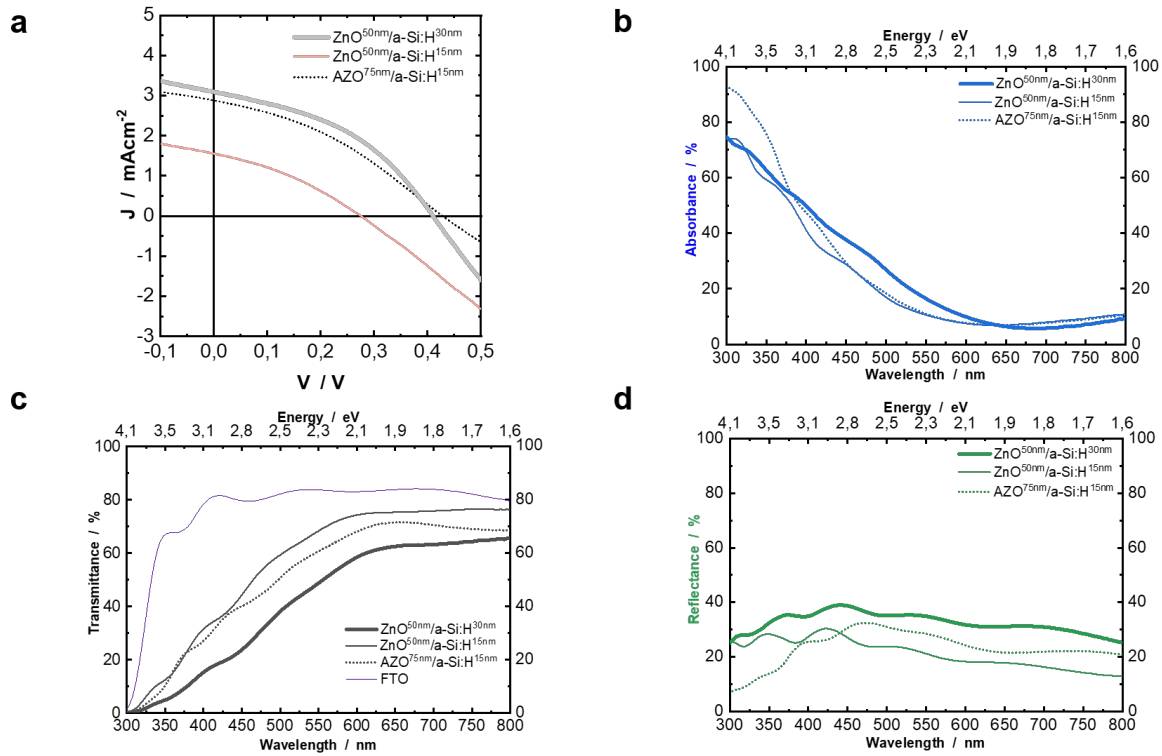


Figure 3. TPV characterization of best devices. a) J-V measurements under AM1.5G illumination of FTO/ZnO(50nm)/a-Si:H(30nm)/MoO₃(10nm)/ITO, FTO/ZnO(50nm)/a-Si:H(15nm)/MoO₃(10nm)/ITO and FTO/AZO(75nm)/a-Si:H(15nm)/MoO₃(10nm)/ITO. b) Absorbance spectra of devices shown in a). c) Transmittance spectra of the glass/FTO substrate, shown as reference, and of whole devices shown in a). d) Reflectance spectra of devices shown in a).

Table 1. Summary of device parameters of absorber thickness variation analysis.

TPV device structure	V_{oc} [V]	J_{sc} [mA cm^{-2}]	FF [%]	PCE [%]
FTO/ZnO(50nm)/a-Si:H(15nm)/MoO ₃ (10nm)/ITO	0.29	1.85	31.0	0.21
FTO/ZnO(50nm)/a-Si:H(30nm)/MoO ₃ (10nm)/ITO	0.41	3.09	41.4	0.51
FTO/ZnO(50nm)/a-Si:H(15nm)/MoO ₃ (20nm)/ITO	0.33	1.86	30.8	0.22
FTO/ZnO (50nm)/a-Si:H(30nm)/MoO ₃ (20nm)/ITO	0.46	3.50	33.4	0.52

Table 2. Summary of main results with TPV parameters of fabricated devices presented in Figure 3.

TPV device structure	CRI	AVT [%]	V_{oc} [V]	J_{sc} [mA cm^{-2}]	FF [%]	PCE [%]	LUE [%]
FTO/ZnO(50nm)/a-Si:H(15nm)/MoO ₃ (10nm)/ITO	89	69	0.29	1.85	31.0	0.21	0.15
FTO/ZnO(50nm)/a-Si:H(30nm)/MoO ₃ (10nm)/ITO	74	50	0.41	3.09	41.4	0.51	0.25
FTO/AZO(75nm)/a-Si:H(15nm)/MoO ₃ (10nm)/ITO	79	62	0.43	2.86	37.0	0.41	0.25

Fabrication of ultrathin a-Si:H/oxide-based transparent solar cells is reported. We study also the effect of using oxide-based carrier selective contacts of ZnO and MoO₃ for electron and hole extraction respectively. We study the effect of varying thickness of ultrathin a-Si:H films on the TPV properties of the devices in terms of AVT and PCE, showing the best results with a 30nm a-Si:H presenting a PCE=0.5% with an AVT=50% and LUE=0.25% and also with a 15nm a-Si:H film we obtain a PCE=0.2% with an AVT=69% and LUE=0.15%. An optimized device is presented showing a PCE=0.4% with an AVT=62% and LUE=0.25%.

Ultrathin a-Si:H/oxide-based solar cells

A.J. Lopez-Garcia, O. Blazquez, C. Voz, J. Puigdollers, V. Izquierdo-Roca, A. Pérez-Rodríguez*

Ultrathin wide-bandgap a-Si:H based solar cells for transparent PV applications

ToC figure

